CHIN. PHYS. LETT. Vol. 38, No. 11 (2021) 117301

Topological Properties in Strained Monolayer Antimony Iodide

Danwen Yuan(袁丹文)[1,2], Yuefang Hu(胡岳芳)[1,2*], Yanmin Yang(杨艳敏)[1,2], and Wei Zhang(张薇)[1,2*]

[1]*Fujian Provincial Key Laboratory of Quantum Manipulation and New Energy Materials, College of Physics and Energy, Fujian Normal University, Fuzhou 350117, China*
[2]*Fujian Provincial Collaborative Innovation Center for Advanced High-field Superconducting Materials and Engineering, Fuzhou 350117, China*

(Received 7 September 2021; accepted 27 September 2021; published online 27 October 2021)

Two-dimensional (2D) topological insulators present a special phase of matter manifesting unique electronic properties. Till now, many monolayer binary compounds of Sb element, mainly with a honeycomb lattice, have been reported as 2D topological insulators. However, research of the topological insulating properties of the monolayer Sb compounds with square lattice is still lacking. Here, by means of the first-principles calculations, a monolayer SbI with square lattice is proposed to exhibit the tunable topological properties by applying strain. At different levels of the strain, the monolayer SbI shows two different structural phases: buckled square structure and buckled rectangular structure, exhibiting attracting topological properties. We find that in the buckled rectangular phase, when the strain is greater than 3.78%, the system experiences a topological phase transition from a nontrivial topological insulator to a trivial insulator, and the structure at the transition point actually is a Dirac semimetal possessing two type-I Dirac points. In addition, the system can achieve the maximum global energy gap of 72.5 meV in the topological insulator phase, implying its promising application at room temperature. This study extends the scope of 2D topological physics and provides a platform for exploring the low-dissipation quantum electronics devices.

DOI: 10.1088/0256-307X/38/11/117301

With the discovery of quantum spin Hall effect (QSHE),[1] numerous researchers turn their attention to two-dimensional (2D) materials with fascinating topological features. Two-dimensional topological insulators (TIs), also called quantum spin Hall insulators, are emerging as novel electronic materials. Such 2D TIs possess an insulating bulk-gap and gapless edge states, which are protected by the time reversal symmetry. These edge states cannot be eliminated by non-magnetic impurities, resulting in robust electronic transport phenomena. Especially, the surface states of three-dimensional (3D) TIs suffer from scattering at any angle except the 180°, while 2D TIs are more likely to realize the conducting channels with low power dissipation than 3D TIs. This makes 2D TIs promising for the study on electron-phonon coupling and potential applications in topological spintronic devices.[2−25] Up to now, several single-layer TIs with single elements have been proposed, such as graphene,[26] stanene,[27] silicene,[28−30] germanene,[28,29] tellurene,[31] selenene,[32] and so on. Moreover, many monolayer binary compounds containing Sb element have also been reported to host a nontrivial topological phase. For example, SbAs,[33] BiSb,[34] and SbS[35] mainly show the honeycomb lattices. However, the QSHE can also be obtained in a square-like lattice.[36] Thus, the topological properties of the monolayer binary compounds of antimony with square lattices still need to be further explored. In order to enrich the physics of 2D materials, it is necessary to design a novel monolayer binary compound with square lattice to realize the topological transport features.

In this Letter, a monolayer binary compound SbI in square lattice is investigated by first-principles calculations. The monolayer SbI shows the buckled square (BS) structural phase and the buckled rectangular (BR) structural phase under different strain levels. When the effects of the spin-orbit coupling (SOC) are considered in the calculations, the monolayer SbI in BR phase undergoes a topological phase transition from a nontrivial TI to a trivial insulator. Meanwhile, the system becomes a Dirac semimetal (DSM) with two equivalent Dirac points at the transition point. These properties make the monolayer SbI an encouraging material for designing novel electronic devices.

Computation Method. The first-principles calculations based on density functional theory (DFT) are performed by the Vienna *ab initio* simulation package (VASP).[37,38] The generalized gradient approximation in the form of Perdew–Burke–Ernzerhof (PBE)[39] is implemented to describe the exchange-correlation energy. The projector augmented wave potentials[40] are used to deal with the electron-ion

Supported by the National Natural Science Foundation of China (Grant Nos. 11974076 and 61804030), and the Key Project of Natural Science Foundation of Fujian Province (Grant No. 2021J02012).
*Corresponding authors. Email: zhangw721@163.com; yuefhu@163.com
© 2021 Chinese Physical Society and IOP Publishing Ltd

interactions. The vacuum space is set to about 20 Å. The positions of all atoms are fully relaxed to ensure that the maximum residual forces are less than 0.001 eV/Å. For self-consistent electronic structure calculation, the K-points mesh is set to be $24 \times 24 \times 1$. The maximally localized Wannier functions[41,42] are generated by the WannierTools[43] and a tight-binding model is established to explicitly calculate the topological features. For interface structure of BR SbI/MgO, the distance between BR SbI and MgO substrate is about 3 Å, and the van der Waals interaction[44–46] is included in the calculations.

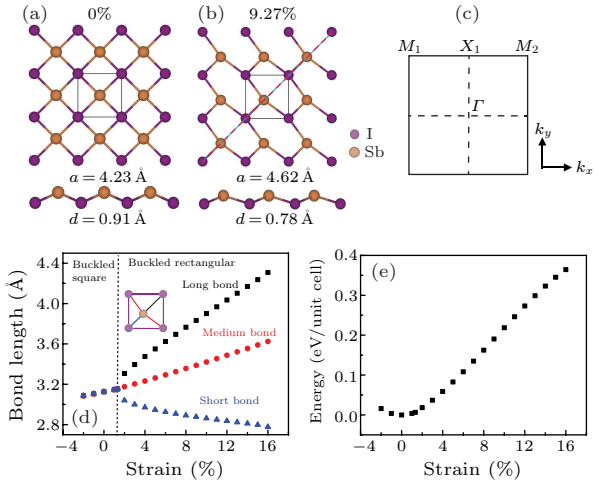

Fig. 1. Top and side views for different structures of the monolayer SbI. (a) Structure without strain in the buckled square phase. (b) Structure under the strain of 9.27% in the buckled rectangular phase. Here, a refers to the lattice constant and d refers to buckling thickness. The red dotted line denotes the mirror-symmetry plane. (c) Two-dimensional Brillouin zone of the monolayer SbI. (d) The variation of bond length with the strain. The inset displays three different lengths of bonds in the monolayer SbI, distinguished by different colors. (e) The variation of energy with the applied strain.

Results and Discussions. We first study the structure of the freestanding monolayer SbI. The optimized structure shows the BS structure, which is the same as those of tellurium[31] and selenium[32] [as displayed in Fig. 1(a)]. The optimized lattice constant is $a_0 = 4.23$ Å. In addition, we find that the buckled structure varies with the applied strain, confirmed by the variation of energy with the applied strain, as presented in Fig. 1(e). The equiaxial strain Δ is defined as $[(a - a_0)/a_0] \times 100\%$ (negative value indicates compression, and positive value indicates expansion). In Fig. 1(e), it shows that as the strain changes from -2% to 10%, the variation of energy is about 220 meV, indicating a phase transition.

According to the applied strain, the monolayer SbI exhibits two structural phases. When $\Delta \leq 1.33\%$, the system shows the BS structure with the space group of P_4/mm (No. 99), and the location of Sb atom is in the lattice center, as displayed in Fig. 1(a). When the strain is greater than 1.33%, the system transits into the BR structure with the space group of Cm (No. 8), and the Sb atom in the lattice center is tilted toward one of the corners [Fig. 1(b)]. The relevant 2D Brillouin zone (BZ) is displayed in Fig. 1(c).

We also investigate the variation of bond lengths with the strain to illustrate the mechanism of the structural phase transition. Actually, according to the different distances between the Sb atom and the neighboring I atom, there are three different lengths of bonds in the monolayer SbI: long bonds, medium bonds and short bonds, as displayed in Fig. 1(d). It is clear that in the BS structure, there are no differences among the three bond lengths, which all increase with the increasing strain. When the strain increases to 1.33%, the differences of bond lengths appear suddenly, indicating a structural phase transition from the BS structural phase to the BR structural phase. As the strain continues to increase, those differences become larger and larger. The above results reveal that the structural phase transition is the first-order transition.

We first focus on the topological properties of the monolayer SbI without strain ($\Delta = 0\%$), which belongs to the BS phase. The electronic band structure without SOC is displayed in Fig. 2(a). We can find that there are energy gaps of 131 meV along the directions of M_1 to Γ and Γ to M_2. However, a degeneracy of valence band and conduction band appears at the X_1 point near the Fermi level. As a result, the monolayer SbI without strain is a semimetal, when excluding SOC. When SOC is considered in the calculations, the energy gaps along those two directions remain, while their values reduce to 84.0 meV. Meanwhile, the degeneracy of bands at the X_1 point is lifted, driving this structure into a trivial topological phase, as plotted in Fig. 2(b).

In the next step, we explore the topological features of the BR structure. In the absence of SOC, the structure under the strain of 9.27% hosts a global energy gap of 76.4 meV, as shown in Fig. 2(c). When the strain of 14.9% is applied, the global non-SOC gap decreases to 0 eV [Fig. 2(e)]. Additionally, as the strain further increases to 15.9%, a band intersection near the Fermi level appears along the Γ to M_2 direction. According to the results of wave-function analysis, the band crossing is protected by the C_s point group,[47] and these bands have different irreducible representations (IRs) of A′ and A″, as shown in the inset of Fig. 2(g). Overall, with the increasing strain, the value of global energy gap gradually increases to 0.11 eV (strain $\Delta = 7.29\%$) at first, then decreases to 0 eV, and remains 0 eV in the strain range from 14.6% to 15.9%. When including SOC, the energy bands of BR structure appear to split due to the Rashba effect, as displayed in Figs. 2(d), 2(f) and 2(h). When the

monolayer SbI is under the strain range from 3.78% to 14.9%, the structure belongs to the nontrivial 2D TI phase. Furthermore, the structure under the strain of 9.27% achieves the maximum global energy gap ∼72.5 meV among the whole 2D TI phase [Fig. 2(d)]. When the strain further increases to 14.9%, there appears a linear band crossing along the M_1–Γ direction, as displayed in Fig. 2(f), indicating the existence of Dirac point. As a matter of fact, there exist two equivalent Dirac points due to the mirror symmetry, whose plane is along the red dotted line in Fig. 1(b). Also, the two Dirac points are illustrated as the red dots in the BZ in Fig. 2(f). Therefore, the structure is actually a DSM. Finally, we can see from Fig. 2(h) that when the strain of 15.9% is applied, an energy gap opens at the band crossing along the Γ–M_2 direction, forming a trivial insulator with a global band gap of 82.7 meV.

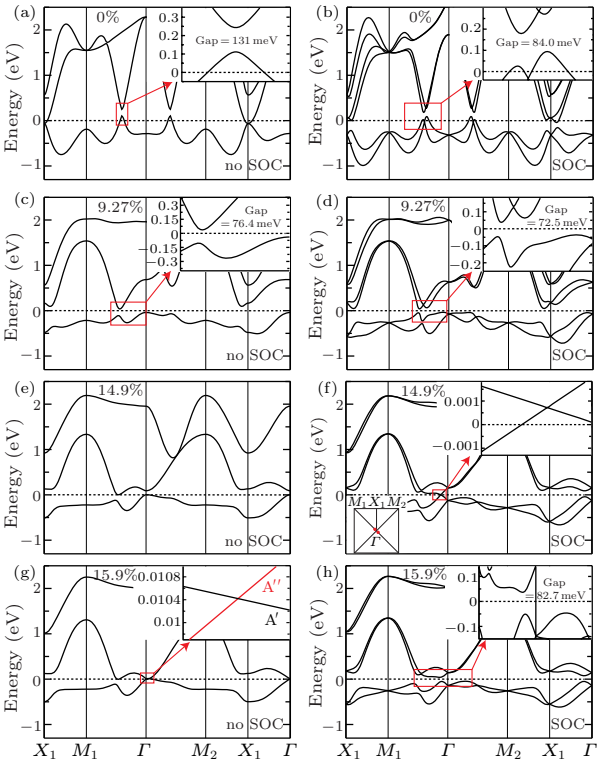

Fig. 2. Without and with SOC band structures for the monolayer SbI under different strain levels: [(a), (b)] $\Delta = 0\%$, [(c), (d)] $\Delta = 9.27\%$, [(e), (f)] $\Delta = 14.9\%$, [(g), (h)] $\Delta = 15.9\%$, respectively. The insets show the enlarged band structures near the Fermi level and a first Brillouin zone. The red dots indicate the locations of the two Dirac points for the structure at 14.9% strain.

When the strain is 9.27%, the structure shows the topological insulating features. By analyzing its evolution of Wannier charge centers (WCC) in an adiabatic pumping process, we calculate the Z_2 invariant to confirm the QSHE of the structure with strain of 9.27% in the BR phase. We can see from Fig. 3(a) that when the structure is under the strain of 9.27%, the crossing number of the reference line (red dashed line) and WCC (black solid lines) is 1, verifying the monolayer SbI in BR phase is a 2D TI. Then, we further calculate the edge states of this structure and the results are shown in Fig. 3(b). The gapless edge states in the bulk gap connect the conduction and valence bands, indicating the nontrivial topological features. It is worth noting that this structure under the strain of 9.27% reaches the maximum global energy gap of 72.5 meV among the whole TI phase, making it a promising material candidate for topological spintronic devices in room temperature.

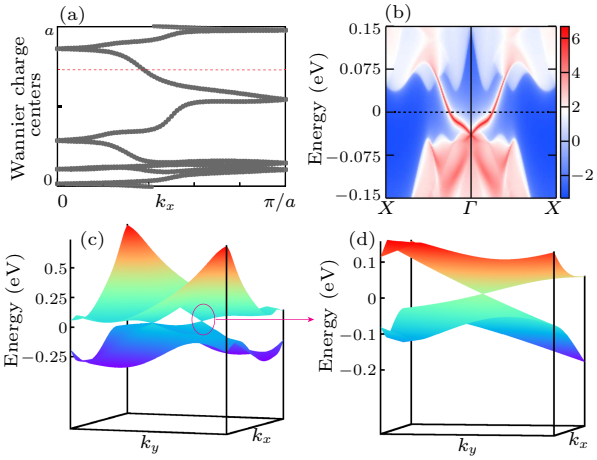

Fig. 3. Topological properties in the buckled rectangular structure for the monolayer SbI. (a) Evolution of the Wannier charge centers along k_x ($\Delta = 9.27\%$). (b) Helical edge states at strain $\Delta = 9.27\%$. (c) Two-dimensional bands under the strain of 14.9%, containing two Dirac points. (d) Enlarged one of the Dirac points ($\Delta = 14.9\%$).

When the strain further increases to 14.9%, a topological phase transition point from nontrivial TI phase to trivial insulator phase appears and the structure turns into a DSM with two Dirac points. Three-dimensional pictures of these Dirac points are displayed in Figs. 3(c) and 3(d). It is clear that a pair of type-I Dirac points are identical owing to the mirror symmetry. Overall, the monolayer SbI in the BR structure maintains in the 2D TI phase in a wide strain range from 3.78% to 14.9%, which implies its potential applications in various situations.

Finally, considering the experimental realization of the topological features in BR structure with the strain of 9.27%, we choose an insulator MgO, which has a large energy gap ∼7.8 eV in experiments,[48] as the substrate candidate to stabilize the strained BR structure. The lattice constant mismatch between the monolayer SbI ($a = 4.23$ Å) and MgO[49] ($a = 4.26$ Å) is small (∼0.7%), making MgO a suitable substrate to grow monolayer SbI. Thus, we investigate the SbI on a strained MgO substrate[50,51] to obtain the QSHE at room temperature. There are two different structures of the BR SbI/MgO system, one of them is the

I atom much closer to the top (001) surface of MgO than the Sb atom, while the other is the Sb atom much closer to the top surface than the I atom. By comparing the energy of these two different structures, we find that the latter one is more stable. Thus, we choose this structure for further study, and its atomic structure is displayed in Fig. 4(a). Figure 4(b) exhibits the projected SOC band structure of the strained BR SbI/MgO system. We can see that the indirect energy gap along M_1 to Γ is 87.0 meV, which is greater than that of the monolayer SbI [Fig. 2(d)] due to the effects of substrate. Moreover, we calculate the Z_2 invariant of the BR SbI/MgO system, and its result is 1, confirming that the topological properties of BR SbI are preserved [Fig. 4(c)]. These results suggest the potential to acquire the topological physics in the monolayer SbI.

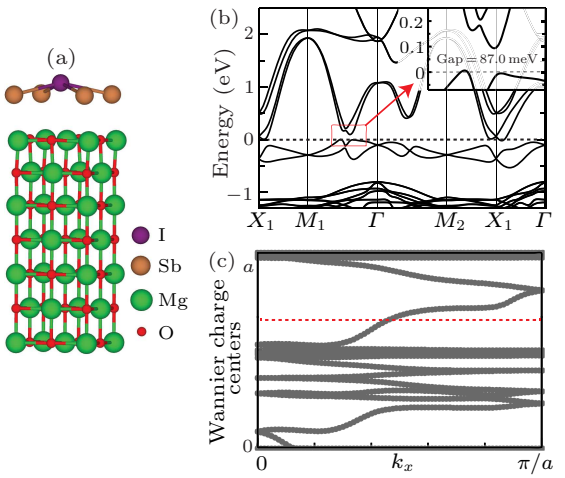

Fig. 4. Topological features of the BR SbI/MgO (001) system with strain. (a) Atomic structure. (b) Projected band structure with SOC. The inset shows the zoom-in band structure along M_1 to Γ. (c) Evolution of the Wannier charge centers along k_x.

In conclusion, based on the first-principles calculations, we propose that a monolayer square SbI hosts a topological phase transition. By applying different levels of strain, the monolayer SbI exhibits two different structural phases, which are the buckled square structure and the buckled rectangular structure. The buckled rectangular SbI exhibits the 2D topological insulating properties over a large strain range from 3.78% to 14.9%. Using hybrid Wannier function technique, we confirm the topological properties of this structure. The maximum global energy gap ~72.5 meV in the whole topological insulator phase is achieved, making this structure favorable for designing topological devices at room temperature. When the strain increases to 14.9%, the structure becomes a DSM, containing two type-I Dirac points. Our study suggests that the topological properties of the monolayer SbI are tunable, making it a promising platform for exploring novel topological physics of low-dimensional materials.

References

[1] Kane C L and Mele E J 2005 *Phys. Rev. Lett.* **95** 226801
[2] Zhang H J, Liu C X, Qi X L, Dai X, Fang Z and Zhang S C 2009 *Nat. Phys.* **5** 438
[3] Zhang J L, Wang D H, Shi M J, Zhu T S, Zhang H J and Wang J 2020 *Chin. Phys. Lett.* **37** 077304
[4] Niu C W, Buhl P M, Bihlmayer G, Wortmann D, Blügel S and Mokrousov Y 2015 *Nano Lett.* **15** 6071
[5] Ma Y D, Kou L Z, Li X, Dai Y and Heine T 2016 *NPG Asia Mater.* **8** e264
[6] Luo W and Xiang H J 2015 *Nano Lett.* **15** 3230
[7] Xu S, Zhou L Q, Wang X Y, Wang H, Lin J F, Zeng X Y, Cheng P, Weng H M and Xia T L 2020 *Chin. Phys. Lett.* **37** 107504
[8] Teshome T and Datta A 2018 *J. Phys. Chem. C* **122** 15047
[9] Guo S D, Mu W Q, Zhu Y T, Wang S Q and Wang G Z 2021 *J. Mater. Chem. C* **9** 5460
[10] Rodin A S, Carvalho A and Castro N A H 2014 *Phys. Rev. Lett.* **112** 176801
[11] Kim J, Baik S S, Ryu S H, Sohn Y, Park S, Park B G, Denlinger J, Yi Y, Choi H J and Kim K S 2015 *Science* **349** 723
[12] Zhang W, Yu R, Feng W X, Yao Y G, Weng H M, Dai X and Fang Z 2011 *Phys. Rev. Lett.* **106** 156808
[13] Yu R, Zhang W, Zhang H J, Zhang S S, Dai X and Fang Z 2010 *Science* **329** 61
[14] Ma F X, Jiao Y L, Gao G P, Gu Y T, Bilic A, Chen Z F and Du A J 2016 *Nano Lett.* **16** 3022
[15] Sui Q, Zhang J X, Jin S H, Xia Y and Li G 2020 *Chin. Phys. Lett.* **37** 097301
[16] König M, Wiedmann S, Brüne C, Roth A, Buhmann H, Molenkamp L W, Qi X L and Zhang S C 2007 *Science* **318** 766
[17] Zhang W, Yu R, Zhang H J, Dai X and Fang Z 2010 *New J. Phys.* **12** 065013
[18] Zhang W, Luo K F, Chen Z D, Zhu Z M, Yu R, Fang C and Weng H M 2019 *npj Comput. Mater* **5** 105
[19] Lv H Z, Wang Z W, Cheng Q B, Zhang W and Yu R 2021 *Phys. Rev. B* **103** L241115
[20] Yang F, Miao L, Wang Z F, Yao M Y, Zhu F F, Song Y R, Wang M X, Xu J P, Fedorov A V, Sun Z, Zhang G B, Liu C H, Liu F, Qian D, Gao C L and Jia J F 2012 *Phys. Rev. Lett.* **109** 016801
[21] Nie S M, Song Z D, Weng H M and Fang Z 2015 *Phys. Rev. B* **91** 235434
[22] Cui Z H, Qian Y T, Zhang W, Weng H M and Fang Z 2020 *Chin. Phys. Lett.* **37** 087103
[23] Sun F, Zhang T, Yi C J, Wu Y L, Zhao H, Wu Q, Shi Y G, Weng H M and Zhao J M 2021 *Phys. Rev. B* **104** L100301
[24] Wu Q, Sun F, Zhang Q Y, Zhao L X, Chen G F and Zhao J M 2020 *Phys. Rev. Mater.* **4** 064201
[25] Sun F, Wu Q, Wu Y L, Zhao H, Yi C J, Tian Y C, Liu H W, Shi Y G, Ding H, Dai X, Richard P and Zhao J M 2017 *Phys. Rev. B* **95** 235108
[26] Yao Y G, Ye F, Qi X L, Zhang S C and Fang Z 2007 *Phys. Rev. B* **75** 041401
[27] Xu Y, Yan B H, Zhang H J, Wang J, Xu G, Tang P Z, Duan W H and Zhang S C 2013 *Phys. Rev. Lett.* **111** 136804
[28] Cahangirov S, Topsakal M, Aktürk E, Sahin H and Ciraci S 2009 *Phys. Rev. Lett.* **102** 236804
[29] Liu C C, Feng W X and Yao Y G 2011 *Phys. Rev. Lett.* **107** 076802
[30] Fabris G S L, Marana N L, Longo E and Sambrano J R 2018 *Theor. Chem. Acc.* **137** 13
[31] Zhang W, Wu Q S, Yazyev O V, Weng H M, Guo Z X, Cheng W D and Chai G L 2018 *Phys. Rev. B* **98** 115411

[32] Chen Z D, Hu Y F, Zhu Z M and Zhang W 2020 *New J. Phys.* **22** 093055
[33] Zhang S L, Xie M Q, Cai B, Zhang H J, Ma Y D, Chen Z F, Zhu Z, Hu Z Y and Zeng H B 2016 *Phys. Rev. B* **93** 245303
[34] Yu W Y, Niu C Y, Zhu Z L, Cai X L, Zhang L W, Bai S Y, Zhao R Q and Jia Y 2017 *RSC Adv.* **7** 27816
[35] Hu X K, Ma Y X, Pang Z X and Li P 2019 *Chem. Phys.* **523** 110
[36] Song Z D, Nie S M, Weng H M and Fang Z 2015 arXiv:1508.05220v1 [cond-mat.mes-hall]
[37] Kresse G and Furthmüller J 1996 *Comp. Mater. Sci.* **6** 15
[38] Kresse G and Furthmuller J 1996 *Phys. Rev. B* **54** 11169
[39] Perdew J P, Burke K and Ernzerhof M 1996 *Phys. Rev. Lett.* **77** 3865
[40] Blöchl P E 1994 *Phys. Rev. B* **50** 17953
[41] Marzari N and Vanderbilt D 1997 *Phys. Rev. B* **56** 12847
[42] Souza I, Marzari N and Vanderbilt D 2001 *Phys. Rev. B* **65** 035109
[43] Wu Q S, Zhang S N, Song H F, Troyer M and Soluyanov A A 2018 *Comput. Phys. Commun.* **224** 405
[44] Thonhauser T, Cooper V R, Li S, Puzder A, Hyldgaard P and Langreth D C 2007 *Phys. Rev. B* **76** 125112
[45] Dion M, Rydberg H, Schröder E, Langreth D C and Lundqvist B I 2004 *Phys. Rev. Lett.* **92** 246401
[46] Luo X, Sullivan M B and Quek S Y 2012 *Phys. Rev. B* **86** 184111
[47] Altmann S L and Herzig P 1994 *Point-Group Theory Tables* (New York: Oxford University Press) p 137
[48] de Boer P K and de Groot R A 1998 *J. Phys.: Condens. Matter* **10** 10241
[49] Baltache H, Khenata R, Sahnoun M, Driz M, Abbar B and Bouhafs B 2004 *Physica B* **344** 334
[50] Yang X, Wang Y, Yan H Y and Chen Y F 2016 *Comput. Mater. Sci.* **121** 61
[51] Odkhuu D 2019 *AIP Adv.* **9** 125129